SIAM J. APPL. MATH.
Vol. 73, No. 2, pp. 974–1001

A MULTIPLE-SCALE ANALYSIS OF EVAPORATION INDUCED MARANGONI CONVECTION*

MATTHEW G. HENNESSY† AND ANDREAS MÜNCH†

Abstract. This paper considers the stability of thin liquid layers of binary mixtures of a volatile (solvent) species and a nonvolatile (polymer) species. Evaporation leads to a depletion of the solvent near the liquid surface. If surface tension increases for lower solvent concentrations, sufficiently strong compositional gradients can lead to Bénard–Marangoni-type convection that is similar to the kind which is observed in films that are heated from below. The onset of the instability is investigated by a linear stability analysis. Due to evaporation, the base state is time dependent, thus leading to a nonautonomous linearized system which impedes the use of normal modes. However, the time scale for the solvent loss due to evaporation is typically long compared to the diffusive time scale, so a systematic multiple scales expansion can be sought for a finite-dimensional approximation of the linearized problem. This is determined to leading and to next order. The corrections indicate that the validity of the expansion does not depend on the magnitude of the individual eigenvalues of the linear operator, but it requires these eigenvalues to be well separated. The approximations are applied to analyze experiments by Bassou and Rharbi with polystyrene/toluene mixtures [*Langmuir*, 25 (2009), pp. 624–632].

Key words. multiple scales, Marangoni convection, slow evaporation

AMS subject classifications. 76E06, 76E17, 34E13

DOI. 10.1137/110849006

1. Introduction.

Convective instabilities play an important role in a number of practical applications and have therefore been the focus of both experimental and theoretical research for many years. The earliest quantitative experiments were undertaken by Bénard [2, 3, 4]. His work inspired Rayleigh [36] to formulate a theory for convective instabilities driven by buoyancy, i.e., by density variations in the liquid that are induced by a thermal gradient. However, experiments by Block [6] and an analytical investigation by Pearson [35] for a one-layer model of a film with a passive gas layer on top and a nondeformable gas/liquid interface showed that the liquid layers in Bénard's experiments were too thin to give rise to buoyancy-driven convection, but that an instability can arise from surface tension variations. These initial investigations have spawned continuing scientific interest in convective instabilities; for an overview of the thriving field, see the review by Bodenschatz, Pesch, and Ahlers [7] and the monographs by Colinet, Legros, and Velarde [12] and Nepomnyaschy, Simanovskii, and Legros [34].

Pearson's analysis assumes a flat interface, and the instability sets in for Marangoni numbers above a critical value. The case of a deformable interface is considered by Scriven and Sternling [40] for a two-layer model; they find it is unstable at all Marangoni numbers with respect to very long waves. Smith [42] shows for a one-layer model in which the inclusion of gravity suppresses the long-wave instability below a nonzero Marangoni number. In fact, Pearson's model is regained in the limit of small capillary and large Galileo number; see Davis [14] or Colinet, Legros, and Velarde

*Received by the editors September 23, 2011; accepted for publication (in revised form) January 2, 2013; published electronically April 23, 2013. This work was supported by King Abdullah University of Science and Technology (KAUST) through award KUK-C1-013-04.
http://www.siam.org/journals/siap/73-2/84900.html
†Mathematical Institute, University of Oxford, 24-29 St. Giles', Oxford OX1 3LB, UK (hennessy@maths.ox.ac.uk, muench@maths.ox.ac.uk).

[12]. In this paper, we will focus on models with nondeformable interfaces.

For an evaporating liquid layer, Marangoni-driven convective instabilities can occur even in the absence of external heating if either the latent heat of evaporation induces a temperature gradient that drives the instability, or the liquid is a mixture with constituents of different volatility and a surface tension that increases as the more volatile species is depleted. In the latter case, the preferred evaporation of one component leads to a concentration gradient which plays a similar role as the temperature gradient. The relevance of compositional Marangoni effects is already discussed by Pearson, but theoretical investigations are less frequent than for the thermocapillary instability, despite the practical importance of the phenomenon in, for example, the preparation of thin polymer films from dilute solutions [8, 19]; we note in passing that solutal Marangoni effects are also thought to play a role in the leveling of drying paint; see Howison et al. [21]. For a system with two layers of solvent/polymer mixtures (with the same solvent but different immiscible polymers in each of the layers), a linear stability analysis is carried out by Souche and Clarke [44]. Recently, Machrafi et al. [30, 29] performed a linear stability analysis for a two-layer model for evaporating water/ethanol mixtures with a flat interface; their approach takes into account the instabilities arising from solutal and thermal Marangoni effects as well as from buoyancy.

An aspect that comes into play for evaporating layers is that the concentration profiles and the layer thickness evolve in time as the volatile component is removed. For the linear stability analysis, this means that the base state which is then perturbed is time dependent; thus the resulting linearized equations have time-dependent coefficients. For such problems, the usual normal-modes approach or generalizations where the spatial and temporal variables can be separated works only in exceptional cases such as in the problem studied by Smolka and Witelski [43] on the extensional motion of a liquid sheet. Floquet theory [5, 37] is designed for time-periodic base flows, which is not the case here. One possible way of handling this difficulty is to circumvent it by modifying the model. This approach was chosen by Souche and Clarke [44], who impose a flux at the lower boundary layer that exactly matches the evaporation at the interface. Thus, the model permits stationary base states, but the modification remains somewhat ad hoc and its impact on the result needs to be assessed.

A general approach is to solve the linearized system numerically as an initial value problem, used by Foster [17] for buoyancy-driven thermal instabilities. For Rayleigh–Marangoni–Bénard convection driven by evaporation, an extension of the amplification method was used by Doumenc et al. [15] and Touazi et al. [45] for a model that includes the temperature gradients induced by the evaporation but not the compositional variations. The results are compared to experiments with polymer solutions by Toussaint et al. [46]. Instead of solving the linearized system for an arbitrary choice of initial perturbation, the optimal choice is determined, which maximizes the amplification of the energy of the perturbation at a given time. The general method was introduced and explored earlier by a number of authors in particular for problems with steady base states but nonnormal linearized operators, where transient amplifications can be larger than the asymptotic behavior indicated by the linear operator's spectrum; see Schmid and Henningson [39] and the references therein. Trouette et al. [47] extend the numerical work to treat the nonlinear model and include other geometries and also stochastic perturbations. Stochastic forcing was treated earlier for convection instabilities in rapidly heated layers by Jhaveri and Homsy [22].

The question naturally arises if the linearized problem can be treated by some analytical approximation. An analytic approach to the initial phase where the base

state changes rapidly but where the gradient is confined to a thin boundary layer was carried out by Kang and Choi [23] for a case of Bénard–Marangoni convection for a horizontal liquid layer that is suddenly cooled from above. They use a propagation method that essentially seeks the solution of the linearized problem in the evolving boundary layer.

On the other hand, after the boundary layer has penetrated the film, the base state often settles into a quasi-equilibrium, where further changes of the gradient are slow compared to the time scale of the instability. For the concentration field, this happens specifically if the solvent loss due to evaporation occurs on a much longer time than diffusion. This has been exploited, for example, by the "frozen time" approach. The time dependence of the coefficients in the linearized equation is neglected but retained for the perturbation itself. This system can be solved by normal modes and the solution will grow or decay depending on the sign of the real part of the leading eigenvalue. This approach has been used by Lick [27] and Currie [13] to investigate thermal convective instabilities (and also by Kang and Choi [23] for late times), and by Machrafi et al. [30, 29] in their work on evaporating water/ethanol mixtures.

In the "frozen time" approach, the eigenvalues are effectively treated as constant, while, in fact, they slowly change as the base state evolves. This implies that it is possible for modes which are initially unstable to stabilize in the long term. It has been repeatedly observed that by integrating the eigenvalue in time and using this as the argument of the exponential function rather than its initial value multiplied by time, an often surprisingly good approximation of the evolution of the perturbation can be obtained. In particular, this approximation is able to capture the change from growth to decay, or vice versa if the leading eigenvalue changes sign. This or similar approximations have been used, for example, by Lick [27], Mahler and Schechter [31], Warner, Craster, and Matar [49], Edmonstone, Craster, and Matar [16], King, Münch, and Wagner [26], and Münch and Wagner [32] for a range of different problems where the base state changes slowly. It is tempting to think that this approximation can be justified by one of the techniques using expansions with multiple time scales as in Kevorkian [24] or Kevorkian and Cole [25]. However, as far as we know, this has not been done for the type of slowly changing base states as they arise in convective instabilities, though we note that multiple scale ideas have been used in the context of boundary layer instabilities where the boundary layer varies slowly in space by, for example, Bouthier [10, 11]. In our paper, we will show how the intuitive result can be recovered from a systematic multiple-scale approach including higher-order corrections that provide insight into the validity of the approximation.

Other approaches that account for the slow change of the base state include, for example, Shen's work [41], which investigates the stability of an incompressible time-dependent flow (inviscid and viscous) by considering the ratio of the kinetic energy of the perturbation velocity field to the energy of the (time-dependent) velocity profile. The derivative of the log of this quantity is then a measure of the growth or decay of the perturbation relative to the base state, and this can be expressed as the sum of the leading "frozen time" eigenvalue and a contribution from the evolving base state. Stability boundaries using energy stability concepts without requiring a separation of time scales were also derived by Homsy [20] for convective instabilities.

The layout of the paper is as follows. In section 2, we formulate a model for an evaporating (laterally infinite) liquid layer consisting of a solution of a nonvolatile polymer in a volatile solvent, with a passive gas on top. We restrict ourselves to the simplest model with a flat, nondeformable interface and where the surface tension is assumed to depend only on the composition. We thus neglect thermal Marangoni as

well as buoyancy effects. Evaporation is assumed to be small on the diffusive time scale, leading to a small Biot number on which the subsequent asymptotic analysis is built. In section 3, we determine asymptotic approximations of the base state to leading order in the Biot number and compare them with numerical results. In section 4, we linearize the model about the full time-dependent base state and then reduce the initial value problem to a finite-dimensional ODE system by projecting it onto the leading modes of the slowly evolving eigenvalue problem. We then exploit the separation of time scales to obtain asymptotic approximations for this system and thus for the full linearized initial value problem via multiple-scale expansions. We also solve the linearized system numerically and compare the solutions with the asymptotic approximations. In section 5, we use our results to discuss the experiments by Bassou and Rharbi [1]. We finally conclude in section 6.

2. Mathematical model.

Governing equations. We consider a liquid film consisting of a mixture of a volatile solvent and a nonvolatile polymer. Coordinates x and z are introduced as shown in Figure 2.1(a), and t represents time. Our focus will be on the onset of the instability via a linear stability analysis, and for this purpose, investigating a spatially two-dimensional model is sufficient. This is different for nonlinear effects, which typically select distinctly three-dimensional hexagonal patterns [1, 4, 38]. Bulk equations for the pressure field $p = p(x, z, t)$, the two components of the velocity $u = u(x, z, t)$ and $w = w(x, z, t)$ (as shown in the sketch), and the concentration of the solvent $c = c(x, z, t)$ consist of the Stokes equations, an incompressibility condition that corresponds to conservation of mass, and a convection/diffusion equation for the concentration field:

$$-\nabla p + \mu \Delta \boldsymbol{u} = 0, \tag{2.1}$$

$$\nabla \cdot \boldsymbol{u} = 0, \tag{2.2}$$

$$c_t + \boldsymbol{u} \cdot \nabla c = D \Delta c, \tag{2.3}$$

where $\boldsymbol{x} = (x, z)$ and $\boldsymbol{u} = (u, w)$, $\nabla = (\partial_x, \partial_z)$ and $\Delta = \nabla^2 = \partial_x^2 + \partial_z^2$. Also, μ is the dynamic viscosity of the liquid and D the diffusion coefficient for the solvent, both of which we assume to be independent of the concentration.

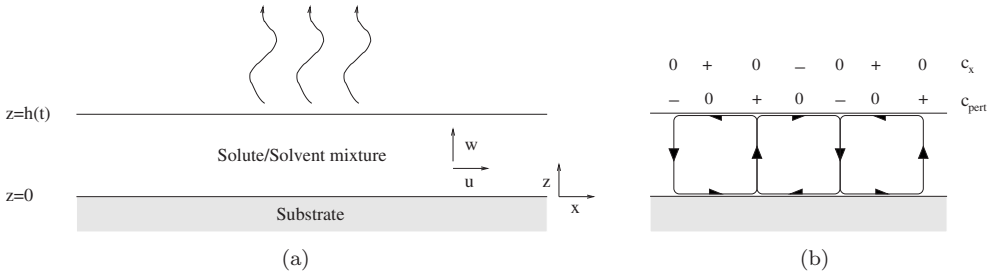

FIG. 2.1. (a) *Sketch of the physical situation with a thin liquid layer consisting of a mixture of a volatile solvent and a nonvolatile polymer.* (b) *Sketch illustrating the basic instability in a two-dimensional setting. Details are given in section* 4.

At $z = 0$, i.e., at the surface of the substrate, we assume no-slip for the horizontal velocity component. Moreover, we assume the substrate is impermeable for both constituents of the fluid, so that

$$\boldsymbol{u} = 0, \qquad c_z = 0. \tag{2.4}$$

We will assume that the interface is nondeformable and thus given as $z = h(t)$. Nondeformability has been frequently used in studies of thermally driven Bénard–Marangoni convection under conditions where surface tension and gravity are strong enough to keep the interface flat [14].

At $z = h(t)$, we impose the kinematic condition and assume that the only volatile component is the solvent, which evaporates from the liquid at a rate that is proportional to its concentration. This simple relation for the evaporation rate is phenomenological and motivated by applications in spin-coating [9]. It was also used by Souche and Clarke in their investigation of Marangoni instabilities for a two-layer film of liquid mixtures with an evaporating solvent [44]. Thus, the boundary conditions are

$$\rho(\boldsymbol{u}\cdot\boldsymbol{e_z} - h_t) = k_m c, \tag{2.5}$$
$$c(\boldsymbol{u}\cdot\boldsymbol{e_z} - h_t) - D\nabla c\cdot\boldsymbol{e}_z = k_m c,$$

where k_m is the mass transfer coefficient (units: length/time). The symbols $\boldsymbol{e_x}$ and $\boldsymbol{e_z}$ denote the unit vectors in the direction of the x and z axis, respectively. We neglect variations of the density between the two species so that the density of the mixture ρ is kept constant. We can eliminate h_t and $\boldsymbol{u}\cdot\boldsymbol{e_z}$ from the second equation with the help of (2.5) and thus replace it by the slightly more compact form

$$D\nabla c\cdot\boldsymbol{e}_z = -k_m(1 - c/\rho)c. \tag{2.6}$$

The concentration gradients along the liquid/air interface induce a Marangoni shear stress,

$$\mu\,\boldsymbol{e_x}\cdot(\nabla\boldsymbol{u} + \nabla\boldsymbol{u}^T)\cdot\boldsymbol{e_z} = -\gamma_c\nabla c\cdot\boldsymbol{e}_x. \tag{2.7}$$

Here, we have assumed that surface tension decreases linearly with increasing concentration of the solvent, so that γ_c is a positive parameter.

Finally, we have initial conditions at $t = 0$,

$$h(0) = h_i, \qquad c(x, z, 0) = c_i(x, z), \tag{2.8}$$

with some specified thickness h_i and initial concentration field c_i. We denote the mean value of the initial concentration field by

$$c_m = \lim_{L\to\infty}\frac{1}{2h_iL}\int_{-L}^{L}\int_0^{h_i} c_i(x, z)dzdx. \tag{2.9}$$

Nondimensionalization. We nondimensionalize the governing equations using the initial film thickness h_i as the length scale for x, z, and h, the diffusive time scale h_i^2/D for t, the ratio of the two, D/h_i, as the velocity scale for u and w, and the pressure scale $\mu D/h_i^2$ for p. For the concentration field, we write $c = c_m + h_i c_s\tilde{c}$, where c_s measures the typical concentration gradient. Notice that for a well-mixed fluid $\tilde{c}_i = 0$. An estimate for the concentration gradient can be obtained from (2.6) if we replace c by its initial mean value c_m, yielding $|c_z| \sim k_m(1 - c_m/\rho)c_m/D \equiv c_s$. With these scalings, we obtain the equations for the bulk (after dropping the tildes from c and c_i),

$$-p_x + u_{xx} + u_{zz} = 0, \tag{2.10a}$$
$$-p_z + w_{xx} + w_{zz} = 0, \tag{2.10b}$$
$$u_x + w_z = 0, \tag{2.10c}$$
$$c_t + uc_x + wc_z = c_{xx} + c_{zz}. \tag{2.10d}$$

For the boundary conditions at $z = 0$ we find

$$u = 0, \qquad w = 0, \qquad c_z = 0, \tag{2.10e}$$

and at the liquid gas interface $z = h(t)$,

$$w - h_t = \delta\beta(1 + \delta(1 - \beta)c), \tag{2.10f}$$

$$c_z = -(1 + \delta(1 - \beta)c)(1 - \delta\beta c), \tag{2.10g}$$

$$u_z + w_x = -\mathrm{Ma}\, c_x; \tag{2.10h}$$

the initial conditions are

$$h(0) = 1, \qquad c(x, z, 0) = c_i(x, z), \tag{2.10i}$$

where the latter is now assumed to have a mean value zero. Three parameters appear in this system:

$$\beta = c_m/\rho, \qquad \delta = \frac{k_m h_i}{D}, \qquad \mathrm{Ma} = \delta\frac{\beta(1 - \beta)\gamma_c \rho h_i}{\mu D}. \tag{2.11}$$

These are the initial solvent volume fraction, the evaporative Biot number, and the Marangoni number, respectively.

To obtain typical values for these parameters, we consider recent experiments by Bassou and Rharbi [1] and find that β is typically around 0.85, while δ is in the range of 0.36 to 0.036 (with the lower values arising for the thinner films) and Marangoni numbers lie between 33 and 2.6×10^3. Details of the computation are given in section 5. This suggests that we can consider the limit of small Biot-number, $0 < \delta \ll 1$, with fixed β and Ma, for all but the thickest films. For most of the computations in sections 3 and 4, we have typically used slightly smaller values for $\delta = 0.01$ and $\beta = 0.3$, but note that this does not affect the results qualitatively. For the comparison of the experiments in section 5, we return to the parameter values that we obtained from Bassou and Rharbi's data.

3. Base state. We seek one-dimensional solutions of (2.10a)–(2.10i), i.e., solutions for which u is zero and w, c, p do not depend on x. We find that $w = 0$, $p = 0$, while $c = C(z, t)$ satisfies a diffusion equation in the bulk,

$$C_t = C_{zz}, \tag{3.1a}$$

and the boundary and initial conditions

$$C_z(0, t) = 0, \tag{3.1b}$$

$$h_t(t) = -\delta\beta(1 + \delta(1 - \beta)C(h(t), t)), \tag{3.1c}$$

$$C_z(h(t), t) = -(1 + \delta(1 - \beta)C(h(t), t))(1 - \delta\beta C(h(t), t)), \tag{3.1d}$$

$$h(0) = 1, \qquad C(z, 0) = 0. \tag{3.1e}$$

In the following, we seek asymptotic solutions to this system of equations for small Biot numbers $\delta \ll 1$ and fixed initial volume fraction β and compare them to numerical solutions. It turns out that we need to consider two time regimes. In the first, the concentration field forms a boundary layer that quickly penetrates the film and then reaches a quasi-equilibrium, while the film thickness remains constant to leading order. In the second, i.e., the slow time regime, the leading-order solution for the thickness and the leading contribution to concentration gradient decrease as a result of the loss of solvent due to evaporation.

3.1. Early time regime $t = O(1)$. Brief inspection of the equations shows that the solution is trivial unless we balance the left- and right-hand sides of (3.1d). We therefore expand C and h as

$$C(z,t) = C_0(z,t) + \delta C_1(z,t) + \cdots, \qquad h(t) = h_0(t) + \delta h_1(t) + \cdots. \tag{3.2}$$

The leading-order problem is

$$C_{0,t} = C_{0,zz}, \tag{3.3a}$$
$$C_{0,z}(0,t) = 0, \tag{3.3b}$$
$$h_{0,t}(t) = 0, \tag{3.3c}$$
$$C_{0,z}(h_0(t),t) = -1, \tag{3.3d}$$
$$h_0(0) = 1, \qquad C_0(z,0) = 0. \tag{3.3e}$$

This shows that in this time regime, h_0 is constant and equal to one, while C_0 satisfies the heat equation and thus can be found by series expansions. Moreover, we can easily see that

$$\int_0^1 C_0(z,t)dz = -t. \tag{3.4}$$

Using this mass-balance relation, (3.3a) and (3.3b), one finds that the long-time asymptotic behavior $t \to \infty$ for the leading-order solution is

$$h_0(t) \sim 1, \qquad C_0(z,t) \sim -z^2/2 + 1/6 - t. \tag{3.5}$$

This will be used to match into the next time regime.

3.2. Late time regime $t = O(\delta^{-1})$. The previous regime breaks down at $t = O(\delta^{-1})$ when evaporation begins to have a significant effect on the film thickness h_0. We rescale $t = \tau/\delta$ and expand

$$C(z,\tau) = \delta^{-1} C_0(z,\tau) + C_1(z,\tau) + \cdots, \qquad h(\tau) = h_0(\tau) + \delta h_1(\tau) + \cdots. \tag{3.6}$$

The leading-order problem is

$$C_{0,zz} = 0, \tag{3.7a}$$
$$C_{0,z}(0,\tau) = 0, \tag{3.7b}$$
$$h_{0,\tau}(\tau) = -\beta\left[1 + (1-\beta)C_0(h_0(\tau),\tau)\right], \tag{3.7c}$$
$$C_{0,z}(h_0(\tau),\tau) = 0, \tag{3.7d}$$
$$h_0 \sim 1, \qquad C_0 \sim -\tau \qquad \text{for } \tau \to 0; \tag{3.7e}$$

the last equation comes from matching to the initial time layer. The solution of (3.7) is

$$C_0(z,\tau) = C_0(\tau), \qquad h_0(\tau) = 1 - \beta\tau - \beta(1-\beta)\int_0^\tau C_0(s)ds, \tag{3.8}$$

with a C_0 that is independent of z. The precise functional form for C_0 needs to be determined from a solvability condition arising from the next-order problem, the relevant parts of which are

$$C_{1,zz} = C_{0,\tau}, \tag{3.9a}$$
$$C_{1,z}(0,\tau) = 0, \tag{3.9b}$$
$$C_{1,z}(h_0(\tau),\tau) = -\left[1 + (1-\beta)C_0(\tau)\right]\left[1 - \beta C_0(\tau)\right]. \tag{3.9c}$$

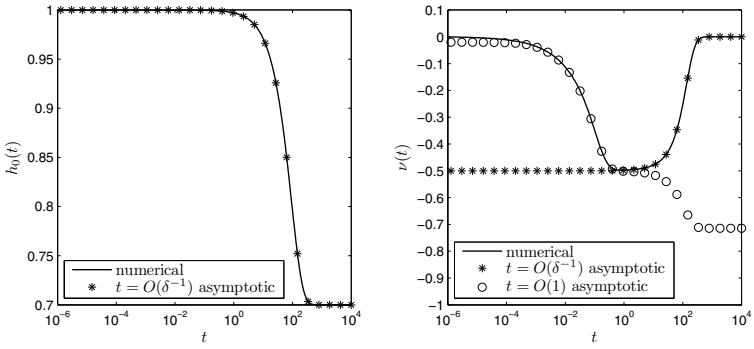

FIG. 3.1. *Comparison of the asymptotic approximations (correct to $O(\delta)$) with numerical solutions of the base state for the full one-dimensional equations* (3.1). *The film thickness is shown on the left and the average concentration gradient (explained in the text) on the right. Note that the leading order for h_0 for $t = O(1)$ is trivial and has therefore been omitted on the left. Parameter values are $\beta = 0.3$ and $\delta = 0.01$.*

Integrating (3.9a) and using (3.7c) to express the resulting right-hand side in terms for $h_{0,\tau}$ yields $(h_0 C_0)_\tau = h_{0,\tau}/\beta$, and therefore

$$C_0 = -\frac{(1-h_0)}{\beta h_0}. \tag{3.10}$$

Using this in (3.7c) gives an ODE for h_0 which has the implicit solution

$$h_0 - 1 + (1-\beta)\ln\left[\frac{h_0 - (1-\beta)}{\beta}\right] = -\tau. \tag{3.11}$$

System (3.9) has the solution

$$C_1(z,\tau) = -\frac{h_0 - 1 + \beta}{2\beta h_0^3}\, z^2 + C_1(0,\tau), \tag{3.12}$$

stated here in terms of h_0. The function $C_1(0,\tau)$ is fixed by a solvability condition for the second-order problem. We do not determine it here since it will not be required for the linear stability analysis in section 4.

We now compare these asymptotic results with numerical results for (3.1) for $\delta = 0.01$ and $\beta = 0.3$. This initial volume fraction of solvent is somewhat small; most physical experiments use solutions where the initial content of polymer is typically on the order of a few percent. The important features of the evolution do not critically depend on the value of β, so we will keep $\beta = 0.3$ for most of this paper. However, in section 5, where we compare our numerical results with experiments by Bassou and Rharbi [1], we will use a β that is much closer to one. Further details for $\beta = 0.85$ can also be found in [18].

In Figure 3.1, we specifically look at the evolution of the film thickness $h(t)$ and the average concentration gradient $\nu(t) = (c(h(t),t) - c(0,t))/h(t)$. We clearly see that for t less than or equal to about one, the film thickness remains approximately constant while the concentration gradient builds up until it plateaus at slightly less than $t = 1$. This in good qualitative and quantitative agreement with the asymptotic solution for the $t = O(1)$ time regime. At later times, in fact shortly after $t = 1$, the

evolution is captured by the asymptotic results of the $t = O(\delta^{-1})$ regime where the film thickness and the concentration change slowly until the solvent reaches depletion at a very late stage. We will exploit this to obtain approximations to the solutions of the linearized equations for small perturbations of the one-dimensional base state in the next section.

4. Linear stability. In the previous section, we have seen that there is no flow in the base state and the concentration field has no lateral variations but a negative gradient in the normal direction. We will now seek to understand how this may change when small perturbations are introduced, reflecting the ubiquitous presence of "noise" in real world systems. We focus on the long-time regime where the base state only changes slowly in time.

For a brief qualitative discussion of the basic instability mechanism, we neglect the change of the base state for the moment. We introduce a perturbation of the concentration field $c_{\text{pert}} = c - C$ along the liquid/air interface (indicated in Figure 2.1(b) by $+$, $-$ signs and 0). As a result, we have lateral concentration gradients c_x that change sign along the interface, and these give rise to Marangoni shear stresses (see (2.10h)) and thus to a Couette-type flow. The direction is such that liquid at the surface is moved away from regions of higher solvent concentration to regions of lower solvent concentration. Mass conservation requires liquid to rise from the bottom to the top in the former instance, which is solvent rich and thus provides a mechanism to overcome the leveling tendencies of diffusion. If this happens in a linearized theory, it typically leads to an exponential growth of the perturbation. Nonlinear effects (for example, from the convection terms in (2.10d)) are expected to eventually put a halt to this growth and typically lead to a hexagonal pattern seen in three-dimensional thermal convection [14], but these are not discussed in this paper. The question remains how the slow change of the base state interacts with the basic instability and how it can be incorporated into the linear stability analysis; this will be addressed in the following sections.

4.1. Formulation. We begin by seeking a solution to the governing equations of the form

$$u(x,z,t) = \alpha \int_{-\infty}^{\infty} \hat{u}(z,t;k) e^{ikx} dk, \tag{4.1a}$$

$$w(x,z,t) = \alpha \int_{-\infty}^{\infty} \hat{w}(z,t;k) e^{ikx} dk, \tag{4.1b}$$

$$p(x,z,t) = \alpha \int_{-\infty}^{\infty} \hat{p}(z,t;k) e^{ikx} dk, \tag{4.1c}$$

$$c(x,z,t) = C(z,t) + \alpha \int_{-\infty}^{\infty} \hat{c}(z,t;k) e^{ikx} dk, \tag{4.1d}$$

$$h(t) = h(t) + \alpha \int_{-\infty}^{\infty} \hat{h}(t;k) e^{ikx} dk, \tag{4.1e}$$

where we assume that $0 < \alpha \ll 1$ so that (4.1) represent a slightly perturbed base state. Since we have assumed that the liquid/air interface remains flat, $\hat{h}(t;k)$ is proportional to a delta function. We are interested in perturbations that can give rize to laterally nontrivial patterns, and therefore restrict our attention to the case $k \neq 0$, where $\hat{h}(t;k)$ is zero.

We insert this ansatz into (2.10) and expand. To $O(1)$, we recover the equations

for the base state (3.1). After eliminating $\hat{u}$, the $O(\alpha)$ equations in the bulk are

$$\hat{p}_{zz} - k^2\hat{p} = 0, \tag{4.2a}$$

$$\hat{w}_{zz} - k^2\hat{w} = \hat{p}_z, \tag{4.2b}$$

$$\hat{c}_t + \hat{w}C_z = \hat{c}_{zz} - k^2\hat{c}, \tag{4.2c}$$

with boundary conditions at $z = 0$,

$$\hat{w} = 0, \quad \hat{w}_z = 0, \quad \hat{c}_z = 0, \tag{4.2d}$$

and at $z = h(t)$,

$$\hat{w} = \delta^2\beta(1-\beta)\hat{c}, \tag{4.2e}$$

$$\hat{c}_z = -\delta\left[1 - 2\beta - 2\delta\beta(1-\beta)C\right]\hat{c}, \tag{4.2f}$$

$$\hat{p}_z = -k^2(\mathrm{Ma} + 2\delta^2\beta(1-\beta))\hat{c}. \tag{4.2g}$$

The initial condition is

$$\hat{c}(z,0;k) = \hat{c}_i(z;k). \tag{4.2h}$$

Also notice that we can solve (4.2a), (4.2b), (4.2d), (4.2e), and (4.2f) for $\hat{w}$ and $\hat{p}$ and that the solution for the former can be written as $\hat{c}(h(t),t)$ times a function of z and of time, say $g(z,\tau;\mathrm{Ma},\delta)$, that is independent of $\hat{c}$. The time dependence of this function enters due to the evolving domain, i.e., via boundary conditions imposed at $z = h$. We do not give the explicit expression for g here, since it is not particularly interesting. With the help of g, we can reduce the linearized problem to one for $\hat{c}$ only:

$$\hat{c}_t(z,t) = \hat{c}_{zz}(z,t) - k^2\hat{c}(z,t) - \hat{c}(h(\tau),t)g(z,\tau;\mathrm{Ma},\delta)C_z(z,\tau), \tag{4.3a}$$

$$\hat{c}_z(0,t) = 0, \tag{4.3b}$$

$$\hat{c}_z(h(\tau),t) = -\delta\left[1 - 2\beta - 2\delta\beta(1-\beta)C(\tau,\delta)\right]\hat{c}(h(\tau),t), \tag{4.3c}$$

$$\hat{c}(z,0) = \hat{c}_i(z). \tag{4.3d}$$

For future reference, we introduce a bulk and a boundary operator, $\mathcal{L}(\tau,\delta)$ and $\mathcal{B}(\tau,\delta)$, respectively, so that (4.3a) can be written as $\hat{c}_t(z,t) = \mathcal{L}(\tau,\delta)\,\hat{c}(z,t)$ and the boundary conditions (4.3b), (4.3c) as $\mathcal{B}(\tau,\delta)\hat{c}(z,t) = 0$.

We finally remark that in a three-dimensional linear stability analysis, the wavenumber is replaced by a wave vector with two components, $\boldsymbol{k} = (k_x, k_y)$. However, only the modulus of the wave vector $(k_x^2 + k_y^2)^{1/2}$ appears in the linearized equations (in place of k), and thus our restriction to a two-dimensional model is done without loss of generality.

4.2. Reduction to a finite-dimensional system. For each wavenumber k, the system (4.3) represents an initial/boundary value problem that is coupled to the initial/boundary value problem for the base state (3.1) and that needs to be solved for any initial perturbation $\hat{c}_i(z)$ and wavenumber k. If the perturbation undergoes sufficient amplification, the base state would be deemed to be unstable with respect to this perturbation. Such a solution can be obtained numerically, but we also seek asymptotic approximations that exploit the slow evolution of the base state in the

time regime $t = O(\delta^{-1})$. For this reason, we have expressed the base state variables C and h in (4.3) in terms of the slow time $\tau = \delta t$.

We now approximate $\hat{c}$ by first expanding in terms of the eigenfunctions of $(\mathcal{L}, \mathcal{B})$ using only the first N leading modes (i.e., the eigenfunctions for the eigenvalues with the largest real part),

$$\hat{c}(z,t) \approx \sum_{j=1}^{N} c_j(t) v_j(z;\tau). \tag{4.4}$$

If the spectrum of the operator is discrete and the eigenfunctions form a complete set, we can expect this representation of $\hat{c}$ to become exact if $N \to \infty$. If the modes included in (4.4) are sufficiently well separated from the neglected part of the spectrum, we will usually only need a few modes to obtain a good approximation of $\hat{c}$ for all but perhaps very early times.

The eigenvalues $\lambda = \lambda_j$ and the eigenfunctions $v = v_j$ satisfy

$$\mathcal{L}(\tau,\delta)\, v = \lambda v, \tag{4.5a}$$

$$v_z = 0 \qquad \text{at } z = 0, \tag{4.5b}$$

$$v_z = -\delta\left[1 - 2\beta - 2\delta\beta(1-\beta)C(\tau,\delta)\right] v \qquad \text{at } z = h(\tau). \tag{4.5c}$$

We assume that the eigenvalues are ordered such that $\Re(\lambda_j) \geq \Re(\lambda_l)$ for $l > j$, where $\Re(\cdot)$ denotes the real part of a complex number. To emphasize that the eigensolutions are parameterized by τ, we will occasionally write $\lambda = \lambda(\tau)$ and $v = v(z;\tau)$.

Let $(\mathcal{L}^*, \mathcal{B}^*)$ denote the adjoint of $(\mathcal{L}, \mathcal{B})$ with respect to the standard inner production (which for two functions f_1 and f_2 is given by integrating $f_1 \bar{f}_2$ with respect to z from 0 to $h(\tau)$, with the bar denoting complex conjugation) and let v_j^* be the adjoint eigenfunctions of $(\mathcal{L}, \mathcal{B})$, i.e., the eigenfunctions of $(\mathcal{L}^*, \mathcal{B}^*)$ for the eigenvalues $\lambda = \lambda_j$. We impose the following normalizations:

$$\int_0^{h(\tau)} |v_j(z;\tau)|^2 dz = 1, \qquad \int_0^{h(\tau)} v_l^*(z;\tau)\bar{v}_j(z;\tau) dz = \delta_{jl}, \tag{4.6}$$

where the bar denotes complex conjugation and δ_{jl} is the Kronecker symbol.

Inserting (4.4) into (4.3a) and then forming inner products with the adjoint eigenfunctions yields the ODE system

$$c_{l,t}(t) - \left(\lambda_l(\tau) + \delta\gamma_{ll}(\tau)\right) c_l(t) = \delta \sum_{j=1, j\neq l}^{N} \gamma_{lj}(\tau) c_j(t) \tag{4.7a}$$

with initial conditions

$$c_l(0) = c_{li} \equiv \int_0^1 v_l^*(z;0)\, \hat{c}_i(z)\, dz \tag{4.7b}$$

for $l = 1, 2, \ldots, N$ and where

$$\gamma_{lj}(\tau) \equiv -\int_0^{h(\tau)} v_l^*(z;\tau)\, \bar{v}_{j,\tau}(z;\tau)\, dz. \tag{4.7c}$$

An alternative expression for the γ_{lj} with $j \neq l$ can be found by taking the derivative of (4.5a) with respect to τ for $\lambda = \lambda_j$ and forming the inner product with v_l^*, leading to

$$\gamma_{lj} = \frac{1}{\lambda_j - \lambda_l} \int_0^{h(\tau)} v_j^*(z)(\mathcal{L}_\tau \bar{v}_l)(z)\, dz. \tag{4.8}$$

For fixed τ and $\delta \to 0$, the operators $\mathcal{L}$ and $\mathcal{B}$ can be expanded as

$$\mathcal{L}(\tau, \delta) = \mathcal{L}_0(\tau) + \delta \mathcal{L}_1(\tau) + \cdots, \tag{4.9a}$$

$$\mathcal{B}(\tau, \delta) = \mathcal{B}_0(\tau) + \delta \mathcal{B}_1(\tau) + \cdots, \tag{4.9b}$$

where we will in particular need the leading-order operators. The expansions start with $O(1)$ terms even though C is $O(\delta^{-1})$; see (3.6). In $\mathcal{B}$, this is offset by a factor of δ^2, and the leading term C_0 does not contribute to $\mathcal{L}$ at all since it does not depend on z (cf. (3.8)). From the expansion for $\mathcal{L}$ and (4.8) we can conclude that the γ_{lj} are $O(1)$ for $l \neq j$, thus ensuring that the equations in (4.7) are indeed only weakly coupled.

4.3. Multiple-scale analysis. The presence of slow and fast time scales allows us to seek asymptotic expansions for the c_l using the "explicit" multiple-scale method [24, 25], where the dependence on the slow time is fixed by eliminating secular terms from higher-order corrections. The situation here differs slightly from the typical application of this method in that the leading-order problem has solutions that decay or grow exponentially rather than being periodic. We will limit our derivation here to the case of two modes $N = 2$ and assume that these two modes are real; numerical inspection of the leading modes for $(\mathcal{L}, \mathcal{B})$ suggests that this is reasonable.

We begin by substituting the ansatz

$$c_j(t) = d_j(T) \exp\left(S_j(t)\right) \tag{4.10}$$

into (4.7) (truncated to two equations for c_1 and c_2), where

$$T \equiv S_1(t) - S_2(t) \tag{4.11}$$

is a new fast time, and

$$S_j(t) \equiv \int_0^{\delta t} \delta^{-1} \lambda_j(\rho) d\rho + \int_0^{\delta t} \gamma_{jj}(\rho) d\rho. \tag{4.12}$$

We obtain

$$d_{1,T}(T) = \frac{\delta \gamma_{12}(\tau)}{\lambda(\tau) + \delta \gamma(\tau)} \exp\left(-T\right) d_2(T), \tag{4.13a}$$

$$d_{2,T}(T) = \frac{\delta \gamma_{21}(\tau)}{\lambda(\tau) + \delta \gamma(\tau)} \exp\left(T\right) d_1(T), \tag{4.13b}$$

$$d_1(0) = c_{1i}, \qquad d_2(0) = c_{2i}, \tag{4.13c}$$

with $\lambda \equiv \lambda_1 - \lambda_2$ and $\gamma \equiv \gamma_{11} - \gamma_{22}$. Since the problem is linear, we may assume, without loss of generality, that (c_{1i}, c_{2i}) have a 2-norm of one, $(c_{1i}^2 + c_{2i}^2)^{1/2} = 1$. Also notice that the eigenvalues of $(\mathcal{L}, \mathcal{B})$ can be expanded as

$$\lambda(\tau) = \lambda^{(0)}(\tau) + \delta \lambda^{(1)}(\tau) + \delta^2 \lambda^{(2)}(\tau) + \cdots \tag{4.14}$$

and that similar expansions can be obtained for the (adjoint) eigenfunctions, the quantities γ, γ_{12}, γ_{21}, and the initial conditions c_{1i} and c_{2i}.

We now expand d_l as

$$d_l(T) = d_l^{(0)}(T,\tau) + \delta d_l^{(1)}(T,\tau) + \delta^2 d_l^{(2)}(T,\tau) + \cdots, \quad l = 1,2, \tag{4.15}$$

and the derivatives as

$$d_{l,T} = d_{l,T}^{(0)} + \delta\left(d_{l,T}^{(1)} + \frac{1}{\lambda^{(0)}} d_{l,\tau}^{(0)}\right) + \delta^2\left(d_{l,T}^{(2)} + \frac{1}{\lambda^{(0)}} d_{l,\tau}^{(1)} - \frac{\lambda^{(1)} + \gamma^{(0)}}{\left(\lambda^{(0)}\right)^2} d_{l,\tau}^{(0)}\right) + \cdots \tag{4.16}$$

and consider the problems for the $d_l^{(n)}$ order by order.

To leading order, we find that $d_1^{(0)} = d_1^{(0)}(\tau)$ and $d_2^{(0)} = d_2^{(0)}(\tau)$ are independent of T and satisfy the initial conditions

$$d_1^{(0)}(0) = c_{1i}^{(0)} \quad \text{and} \quad d_2^{(0)}(0) = c_{2i}^{(0)}. \tag{4.17}$$

The functions $d_l^{(0)}(\tau)$, $l = 1,2$, are determined by considering the next-order problem, which is

$$d_{1,T}^{(1)}(T,\tau) = \frac{\gamma_{12}^{(0)}(\tau)}{\lambda^{(0)}(\tau)} \exp(-T) d_2^{(0)}(\tau) - \frac{d_{1,\tau}^{(0)}(\tau)}{\lambda^{(0)}(\tau)}, \tag{4.18a}$$

$$d_{2,T}^{(1)}(T,\tau) = \frac{\gamma_{21}^{(0)}(\tau)}{\lambda^{(0)}(\tau)} \exp(T) d_1^{(0)}(\tau) - \frac{d_{2,\tau}^{(0)}(\tau)}{\lambda^{(0)}(\tau)}, \tag{4.18b}$$

$$d_1^{(1)}(0,0) = c_{1i}^{(1)}, \qquad d_2^{(1)}(0,0) = c_{2i}^{(1)}. \tag{4.18c}$$

The last terms in (4.18a) and (4.18b) are capable of introducing secular terms to the corrections and therefore need to be eliminated. This implies that $d_1^{(0)}$ and $d_2^{(0)}$ are also constant in τ, and thus

$$d_1^{(0)} = c_{1i}^{(0)}, \qquad d_2^{(0)} = c_{2i}^{(0)}. \tag{4.19}$$

We wish to carry the approximation one order further and integrate (4.18), which introduces two new τ-dependent constants that are determined by eliminating secular terms from the second-order correction problem. The details of this calculation are given in the appendix. The result yields the following approximation for c_1 and c_2:

$$\begin{aligned} c_1(t) &= c_{1i}^{(0)} \exp(S_1(t)) - \delta \frac{\gamma_{12}^{(0)}(\tau)}{\lambda^{(0)}(\tau)} \exp(S_2(t)) c_{2i}^{(0)} \\ &\quad + \delta\left[c_{1i}^{(1)} + c_{1i}^{(0)} \int_0^\tau \frac{\gamma_{12}^{(0)}(\rho)\gamma_{21}^{(0)}(\rho)}{\lambda^{(0)}(\rho)} d\rho + \frac{\gamma_{12}^{(0)}(0)}{\lambda^{(0)}(0)} c_{2i}^{(0)}\right] \exp(S_1(t)), \end{aligned} \tag{4.20a}$$

$$\begin{aligned} c_2(t) &= c_{2i}^{(0)} \exp(S_2(t)) + \delta \frac{\gamma_{21}^{(0)}(\tau)}{\lambda^{(0)}(\tau)} \exp(S_1(t)) c_{1i}^{(0)} \\ &\quad + \delta\left[c_{2i}^{(1)} + c_{2i}^{(0)} \int_0^\tau \frac{\gamma_{12}^{(0)}(\rho)\gamma_{21}^{(0)}(\rho)}{-\lambda^{(0)}(\rho)} d\rho + \frac{\gamma_{21}^{(0)}(0)}{-\lambda^{(0)}(0)} c_{1i}^{(0)}\right] \exp(S_2(t)). \end{aligned} \tag{4.20b}$$

A first comment refers to the elimination of secular terms. The rational basis for this is that these terms break the ordering of the asymptotic expansion in the limit $\delta \to 0$ for fixed τ. It turns out that the secular terms induced by the unknown functions in τ that arise when solving for $d_1^{(0)}$ and $d_1^{(1)}$ yield contributions that are asymptotically comparable to the lower-order terms for $\delta \to 0$, τ fixed, and therefore need to be eliminated. This does not work for $d_2^{(0)}(\tau)$, for example, since the first term in (A.4b) still yields an $O(\delta)$ contribution in the expansion for d_2 that dominates the leading-order (i.e., $O(1)$) term as $\delta \to 0$, with τ fixed.

This highlights an underlying problem with the expansions that can also be seen in the final result (4.20) for c_1 and c_2. Even though we have eliminated all secular terms, the resulting expansion for the second component becomes inconsistent for large t. Specifically, the second term in the first line of (4.20b) dominates the leading-order term in the first line as $t \to \infty$. The inconsistency can be avoided by comparing magnitudes of both components together, for example, by comparing their 2-norm $(c_1^2 + c_2^2)^{1/2}$, rather than for the individual components. Then the expansion for (c_1, c_2) appears to be consistent as long as the initial value $c_{1i}^{(0)}$ is not zero (or if all contributions from $\exp(S_1(t))$ vanish for a special choice of initial conditions), which is the most important case.

Returning to the secular terms in the expansion for (d_1, d_2) with the corresponding weighted norm $(d_1^2 + (d_2 \exp(-T))^2)^{1/2}$ shows that the secular terms arising in $d_1^{(0)}$ and $d_1^{(1)}$ make the expansion inconsistent and need to be eliminated. For $d_2^{(0)}$ and $d_2^{(1)}$, a similar argument can be made only if the initial conditions are specially chosen so that the terms $\exp(T)$ are not present.

Notice that the $O(\delta)$ corrections in the coefficients of the exponentials in (4.20) are divided by the difference of the first and second eigenvalues. This emphasizes the importance of maintaining an $O(1)$ gap between these two eigenvalues in particular as $\delta \to 0$; double or nearly double eigenvalues require a separate discussion. On the other hand, no restriction seems to be required for the individual eigenvalues, so that the expansion remains valid even near stability transitions, i.e., where $|\lambda_1|$ becomes small.

We can now insert (4.20) into the two-mode truncation of (4.4) to obtain an approximation for $\hat{c}$. For $t \to \infty$, only the terms proportional to $\exp(S_1(t))$ survive, and thus

$$\begin{aligned}\hat{c}(z,t) \approx \Bigg\{ & c_{1i}^{(0)} v_1(z;\delta t) + \delta \left[c_{1i}^{(1)} + c_{1i}^{(0)} \int_0^{\delta t} \frac{\gamma_{12}^{(0)}(\rho)\gamma_{21}^{(0)}(\rho)}{\lambda^{(0)}(\rho)} d\rho + \frac{\gamma_{12}^{(0)}(0)}{\lambda^{(0)}(0)} c_{2i}^{(0)} \right] v_1(z;\delta t) \\ & + \delta c_{1i}^{(0)} \frac{\gamma_{21}^{(0)}(\delta t)}{\lambda^{(0)}(\delta t)} v_2(z;\delta t) + O(\delta^2) \Bigg\} \exp\left[\int_0^{\delta t} \delta^{-1}\lambda_1(\rho) + \gamma_{11}(\rho) d\rho \right].\end{aligned} \tag{4.21}$$

This result suggests a straightforward generalization to the case with a general number of N modes (for a detailed derivation, see [18]):

$$\begin{aligned}\hat{c}(z,t) \approx \Bigg\{ & c_{1i}^{(0)} v_1(z;\delta t) + \delta c_{1i}^{(1)} v_1(z;\delta t) \\ & + \delta \sum_{l=2}^{N} \left[c_{1i}^{(0)} \int_0^{\delta t} \frac{\gamma_{1l}^{(0)}(\rho)\gamma_{l1}^{(0)}(\rho)}{\lambda_1^{(0)}(\rho) - \lambda_l^{(0)}(\rho)} d\rho + \frac{\gamma_{1l}^{(0)}(0)}{\lambda_1^{(0)}(0) - \lambda_l^{(0)}(0)} c_{li}^{(0)} \right] v_1(z;\delta t) \\ & + \delta c_{1i}^{(0)} \sum_{l=2}^{N} \frac{\gamma_{l1}^{(0)}(\delta t)}{\lambda_1^{(0)}(\delta t) - \lambda_l^{(0)}(\delta t)} v_l(z;\delta t) + O(\delta^2) \Bigg\} \exp\left[\int_0^{\delta t} \delta^{-1}\lambda_1(\rho) + \gamma_{11}(\rho) d\rho \right].\end{aligned} \tag{4.22}$$

If we take $N \to \infty$, we see that the corrections remain small, provided the two infinite series that arise in (4.22) converge (for fixed time). The terms in the first series have denominators that are the distance of the first eigenvalue from the lth eigenvalue. Motivated by the theory for Sturm–Liouville problems, we would expect that $|\lambda_l| = O(l^2)$ for $l \to \infty$. Our numerical trials confirm that this is indeed the case for the eigenvalues of (4.5). Moreover, these trials suggest that the γ_{l1} remain bounded as l increases, and therefore we can expect the first series to converge for appropriately normalized initial data $c_{li}^{(0)}$. A similar argument can be made for the second sum in (4.22), i.e., in the bottom line.

4.4. Comparison with numerical solutions. We now compare the asymptotic approximations obtained in the previous section with numerical solutions of (4.3). For this we introduce two ways to truncate (4.21) which approximate $\hat{c}$ with a different degree of accuracy. The first, or basic, approximation retains only the leading-order-in-δ behavior in all its constituents (exponents and prefactors),

$$\hat{c}_{\mathrm{bas}}(z,t) = c_{1i}^{(0)} v_1^{(0)}(z;\delta t) \exp\left[\int_0^{\delta t} \delta^{-1}\lambda_1^{(0)}(\rho) d\rho\right], \tag{4.23a}$$

$$c_{1i}^{(0)} = \int_0^1 v_1^{*(0)}(z;0)\, \hat{c}_i(z)\, dz, \tag{4.23b}$$

where ${v_1}^{(0)}$ and $v_1^{*(0)}$ is the leading-order part of the δ-expansion for the first eigenfunction and for the first adjoint eigenfunction, respectively. The second, improved one uses the full eigenvalues and (adjoint) eigenfunctions of the operator $\mathcal{L}$ instead of the leading-order approximations,

$$\hat{c}_{\mathrm{imp}}(z,t) = c_{1i} v_1(z;\delta t) \exp\left[\int_0^{\delta t} \delta^{-1}\lambda_1(\rho) + \gamma_{11}(\rho) d\rho\right], \tag{4.24a}$$

$$c_{1i} = \int_0^1 v_1^{*}(z;0)\, \hat{c}_i(z)\, dz. \tag{4.24b}$$

All these approximations and the numerical solution depend on the base state either through the coefficients of the system of differential equations or through quantities such as the function $\lambda_1(\tau)$, $\gamma_{11}(\tau)$, etc. Since the multiple-scale expansion relies on the slow evolution of this base state, we skip the transient initial phase. Therefore, in all cases except one (highlighted explicitly later in this section), we use the two-term approximation $C(z,\tau) = \delta^{-1}C_0(\tau) + C_1(z,\tau)$ from the expansion for the long-time evolution for C (section 3.2) as the base state.

The approximation $\hat{c}_{\mathrm{bas}}$ has the advantage that the τ-dependence of the coefficients can be easily scaled out of the leading-order eigenproblem. To see this, we return to the formulation (4.2) of the eigenproblem, take the leading-order problem, and rescale according to

$$z = h_0\,\check{z}, \quad \lambda^{(0)} = h_0^{-2}\,\check{\lambda}, \quad k = h_0^{-1}\check{k}, \quad \hat{c}^{(0)} = \check{c},$$
$$\hat{p}^{(0)} = \frac{\beta h_0^{-1}\check{p}}{h_0 - 1 + \beta}, \quad \hat{w}^{(0)} = \frac{\beta\check{w}}{h_0 - 1 + \beta}, \quad \mathcal{M} = \frac{h_0 - 1 + \beta}{\beta}\,\mathrm{Ma}. \tag{4.25}$$

As a result, we obtain the equations in the bulk,

$$\check{p}_{\check{z}\check{z}} - \check{k}^2\check{p} = 0, \qquad \check{w}_{\check{z}\check{z}} - \check{k}^2\check{w} = \check{p}_{\check{z}}, \qquad \check{\lambda}\check{c} - \check{z}\check{w} = \check{c}_{\check{z}\check{z}} - \check{k}^2\check{c}, \tag{4.26a}$$

and the boundary conditions

$$\check{w} = 0, \quad \check{w}_z = 0, \quad \check{c}_z = 0 \qquad \text{at } \check{z} = 0, \tag{4.26b}$$

$$\check{w} = 0, \quad \check{c}_z = 0, \quad \check{p}_z = -\check{k}^2 \mathcal{M} \check{c} \qquad \text{at } \check{z} = 1. \tag{4.26c}$$

As τ changes, $\check{k}$ and $\mathcal{M}$ change if k and Ma are kept fixed, so we need to solve (4.26) for all values of $\check{k}$ and $\mathcal{M}$. If we use the notation $\check{\lambda}_1 = \check{\lambda}_1(\check{k}, \mathcal{M})$ and $\check{v}_1 = \check{v}_1(\check{z}; \check{k}, \mathcal{M})$ to make the dependence of the eigensolution (here for the top eigenvalue and eigenfunction) on $\check{k}$ and $\mathcal{M}$ explicit, we can express $\lambda_1^{(0)}$ and $v_1^{(0)}(z;\tau)$ as

$$\lambda_1^{(0)}(\tau) = h_0(\tau)^{-2} \check{\lambda}_1 \left(h_0(\tau) k, \frac{h_0 - 1 + \beta}{\beta} \mathrm{Ma} \right), \tag{4.27a}$$

$$v_1^{(0)}(z;\tau) = \check{v}_1 \left(\frac{z}{h_0(\tau)}; h_0(\tau) k, \frac{h_0 - 1 + \beta}{\beta} \mathrm{Ma} \right), \tag{4.27b}$$

and then use these in (4.23). After that we can eliminate the dependence on $h_0(\tau)$ from the integrand in the exponential by choosing $\eta = h_0$ as the new integration variable, so that

$$c_{\mathrm{bas}}(z,t) = c_{1i}^{(0)} v_1^{(0)}(z;\tau) \exp\left(I/\delta\right), \quad I = \int_{h_0(\tau)}^{1} \frac{\check{\lambda}_1 \left(\eta k, \frac{\eta - 1 + \beta}{\beta} \mathrm{Ma} \right)}{\eta(\eta - 1 + \beta)} d\eta. \tag{4.28}$$

We now collect some properties of (4.26). The problem corresponds to the insulating case in Pearson's work [35] on thermal Bénard–Marangoni convection. An argument by Lin [28] can be used to show that the spectrum of this problem consists exclusively of discrete eigenvalues $\check{\lambda}$. Vrentas and Vrentas [48] proved that when an eigenvalue crosses a stability boundary its real part changes sign and the imaginary part vanishes. Furthermore, we numerically inspected the top ten eigenvalues $\check{\lambda}_n$ (ordered according to their real part) for a range of wavenumbers $\check{k}$ and Marangoni numbers $\mathcal{M}$. These eigenvalues were always real, i.e., the imaginary part was numerically zero, and the behavior for large n was found to be $\lambda_n^{(0)} = O(n^2)$. The eigenvalues appeared to remain separated for all values of $\mathcal{M}$ and $\check{k}$ we inspected. For the full eigenproblem (i.e., for $(\mathcal{L}, \mathcal{B})$) these properties can either be inferred by perturbation arguments or probed for plausibility by numerical computations.

Returning to the leading-order eigenproblem, Figure 4.1(a) describes the situation for the top eigenvalue $\check{\lambda}_1$ in the $(\check{k}, \mathcal{M})$ plane. The plane is split into two regions where $\check{\lambda}_1$ is either positive or negative; the line separating the two regions represents the cutoff wavenumber $\check{k}_{\mathrm{cut}}(\mathcal{M})$ for each value of $\mathcal{M}$ and is characterized by the condition that $\check{\lambda}_1$ is zero there. Above the line, the eigenvalue is positive, and below, it is negative; it ends at $\check{k} = 0$ at the critical Marangoni number $\mathcal{M}_c$. The value for $\mathcal{M}_c$ can be found from a small k expansion to be $\mathcal{M}_c = 80$. The implication is that for each $\mathcal{M} > \mathcal{M}_c$, the top eigenvalue is positive for a range of wavenumbers $0 < \check{k} < \check{k}_{\mathrm{cut}}$ and negative for larger $\check{k}$. We remark in passing that for fixed $\mathcal{M}$, the eigenvalue achieves its largest positive value for a wavenumber $\check{k}_m$ that by numerical inspection is found to be typically order one or larger except if $\mathcal{M}$ is (very) close to $\mathcal{M}_c$. For Marangoni numbers below $\mathcal{M}_c$, all eigenvalues are negative.

Our goal is to compare the approximations (4.23) and (4.24) with numerical solutions for (4.3) by choosing an initial perturbation and then comparing the amplification that is achieved. For the numerical solution and for each of the approximations,

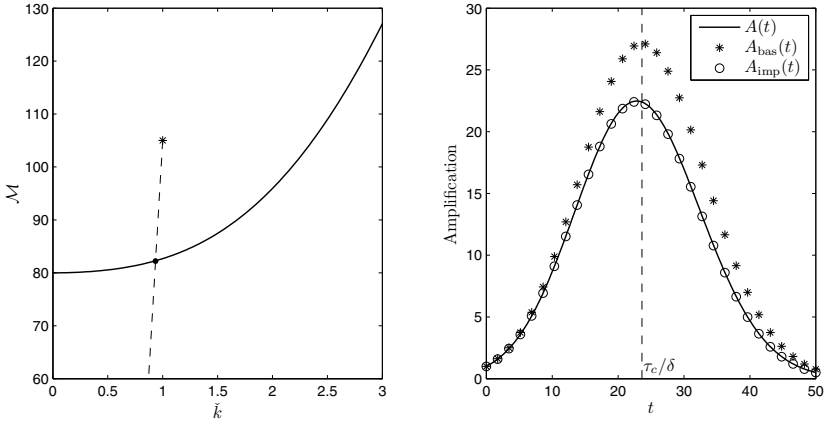

(a) (b)

FIG. 4.1. (a) *Regions where the top eigenvalue of the leading-order part of the operator $\mathcal{L}$ are positive or negative (above and below the solid line). The dashed line shows the values of $\check{k}$ and $\mathcal{M}$ that are traversed for the fixed values of k and Ma used by the numerical computations* (4.32). *The star emphasizes the initial value for $\check{k}$ and $\mathcal{M}$, and the bullet denotes the intersection with the boundary between the two regions. Further explanations are given in the text.* (b) *Comparison of the amplification obtained for the numerical solution of the exact linearized problem with those for the asymptotic approximations. The initial perturbation was the eigenfunction associated with the top eigenvalue for $\mathcal{L}$ at $\tau = 0$. Further explanations including the definition of the amplifications are given in the text.*

the amplification is defined by

(4.29)
$$A(t) = \frac{\max_z |\hat{c}(z,t)|}{\max_z |\hat{c}(z,0)|}, \quad A_{\rm bas}(t) = \frac{\max_z |\hat{c}_{\rm bas}(z,t)|}{\max_z |\hat{c}(z,0)|}, \quad A_{\rm imp}(t) = \frac{\max_z |\hat{c}_{\rm imp}(z,t)|}{\max_z |\hat{c}(z,0)|},$$

respectively. Note that the denominator is the same in all three expressions; as a result, the initial amplification does not need to be one for $A_{\rm bas}$ and $A_{\rm imp}$. From (4.23a) and (4.24) we obtain

$$A_{\rm bas}(t) = |c_{1i}^{(0)}| \frac{\max_z |v_1^{(0)}(z;\tau)|}{\max_z |\hat{c}(z,0)|} \exp\left[\int_0^{\delta t} \delta^{-1} \lambda_1^{(0)}(\rho) d\rho\right], \tag{4.30a}$$

$$A_{\rm imp}(t) = |c_{1i}| \frac{\max_z |v_1(z;\tau)|}{\max_z |\hat{c}(z,0)|} \exp\left[\int_0^{\delta t} \delta^{-1} \lambda_1(\rho) + \gamma_{11}(\rho) d\rho\right]. \tag{4.30b}$$

For our first set of comparisons, we pick the eigenfunction of the top eigenvalue for the full operator $\mathcal{L}$ with $\tau = 0$ as initial condition,

$$\hat{c}_i(z) = \frac{v_1(z;0)}{\max_z |v_1(z;0)|}, \tag{4.31}$$

which we have normalized here with respect to the maximum norm for definiteness. For (4.31), c_{1i} and $c_{1i}^{(0)}$ are equal to one and c_{2i} and $c_{2i}^{(0)}$ are zero.

For the numerical solution of the linearized system (4.3) and also for the asymptotic results, we use the long-time approximation (3.6) of the base state retaining the first two terms for C and the leading-order term for h, and set $C_1(0,\tau) = 1/6$ in (3.12).

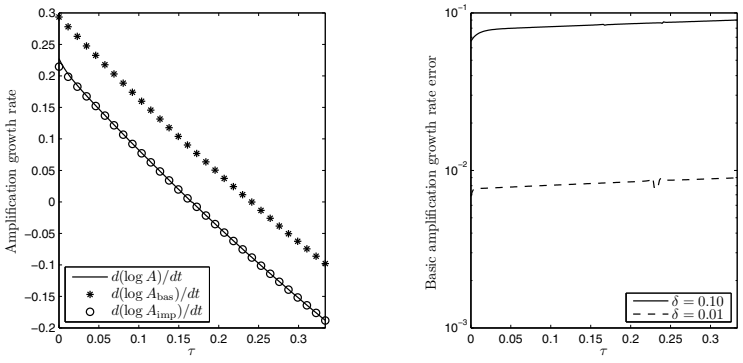

(a) (b)

FIG. 4.2. (a) *Comparison of the growth rate of the log of the three types of amplifications defined in* (4.29) *for* $\delta = 0.1$. (b) *The absolute value of the difference between the growth rate of the log of* A *and the basic asymptotic approximation* A_{bas} *for two different values of* δ.

The resulting operator $(\mathcal{L}, \mathcal{B})$ is only correct to leading order, but for comparing the results of the three solutions/approximations it is sufficient to be consistent and use the same base state for all of them.

Furthermore, we use the following parameters:

$$\delta = 0.01, \qquad \beta = 0.3, \qquad \mathrm{Ma} = 105, \qquad k = 1. \tag{4.32}$$

The path described by $\check{k}$ and $\mathcal{M}$ in the $(\check{k}, \mathcal{M})$ plane for these values of k and Ma as the base state slowly changes is indicated in Figure 4.1(a) by a dashed line, with the initial value (k, Ma) indicated by a star. The point where the line intersects the line $\check{\lambda} = 0$ is emphasized by a bullet; let τ_c denote the value of the slow time variable at which this happens. For $\tau < \tau_c$, the exponential factor in (4.23a) grows, and it decays for $\tau > \tau_c$, as shown in Figure 4.1(b). This is in good agreement with the time at which A_{imp} and A achieve their maximum. Also, the value of the maximum amplification A_{imp} and A agree very well, while for A_{bas}, we note a discrepancy of about 20%.

For closer verification of our asymptotic results, and to better understand the origin of the deviation for A_{bas}, we compare the time derivative of the log of A, A_{bas}, and A_{imp}. In Figure 4.2(a), we chose a value of $\delta = 0.1$ that is considerably larger than previously, because otherwise the lines would be hard to distinguish on the scale of the figure. At this value of δ, $d\log(A(t))/dt$ agrees very well with $d\log(A_{\mathrm{imp}}(t))/dt$ but somewhat less well with $d\log(A_{\mathrm{bas}}(t))/dt$—the absolute value here is about 0.07, which corresponds to a relative error of 33% compared to the value of $d\log(A(t))/dt$ at $t = 0$.

However, the deviation is expected and is a result of the poorer approximation for the eigenvalue and the omission of the γ_{11} in (4.30a). The difference between these quantities is approximately

$$d\log(A_{\mathrm{imp}})/dt - d\log(A_{\mathrm{bas}})/dt \approx \lambda_1 - \lambda_1^{(0)} + \delta\gamma_{11}.$$

This suggests an $O(\delta)$ error in $d\log(A_{\mathrm{bas}}(t))/dt$. Indeed, as Figure 4.2(b) shows, the absolute error $d\log(A_{\mathrm{bas}}(t))/dt - d\log(A(t))/dt$ goes down by a factor of ten as we decrease δ from 0.1 to 0.01.

To recover an estimate for the relative error in A_{bas} at the time of maximum amplification $t_c = \tau_c/\delta$, we need to integrate and exponentiate the previous expression, so that

$$\left|\frac{A_{\text{bas}} - A_{\text{imp}}}{A_{\text{imp}}}\right| \approx \left|\exp\left[-\int_0^{\tau_c/\delta} \lambda_1(\rho) - \lambda_1^{(0)}(\rho) + \delta\gamma_{11}(\rho)\,d\rho\right] - 1\right|,$$

where we have used A_{imp} as a reference value instead of the numerical solution A. The value in the integrand is, as we have argued, $O(\delta)$, so that the integral is an $O(1)$ value times τ_c. In fact, the value of the integral is -0.19; thus the right-hand side evaluates to $|\exp(0.19) - 1| = 0.21$, i.e., an error of 21%, which agrees well with what we observed for the graphs in Figure 4.1(b). This result implies that the deviation of the maximum of A_{bas} from the maximum of A cannot be decreased by a smaller δ, but only by using better approximations for the eigenvalue and including the γ_{11} term. On the other hand, for some practical applications, even an error of 20% or more may be acceptable, so that the maximum of A_{bas} would be a sufficiently good approximation, provided τ_c is not too large.

Next we consider the projection onto the eigensolutions and compare

$$c_j(t) = \int_0^{h(\tau)} v_j^*(z;\tau)\,\hat{c}(z,\tau)\,dz$$

with

$$c_1(t) = \left\{1 + \delta\int_0^{\delta t} \frac{\gamma_{12}(\rho)\gamma_{21}(\rho)}{\lambda(\rho)}d\rho\right\}\exp\left[\int_0^{\delta t} \delta^{-1}\lambda_1(\rho) + \gamma_{11}(\rho)d\rho\right], \tag{4.33a}$$

$$c_2(t) = \delta\frac{\gamma_{21}(\tau)}{\lambda(\tau)}\exp\left[\int_0^{\delta t} \delta^{-1}\lambda_1(\rho) + \gamma_{11}(\rho)d\rho\right]$$

$$- \delta\frac{\gamma_{21}(0)}{\lambda(0)}\exp\left[\int_0^{\delta t} \delta^{-1}\lambda_2(\rho) + \gamma_{22}(\rho)d\rho\right]. \tag{4.33b}$$

The graphs coincide perfectly in Figure 4.3, thus verifying in particular the $O(\delta)$ contribution to c_2.

We now turn to more generic initial data for the perturbation

$$c_i(z) = 16z^2(1-z)^2 \tag{4.34}$$

when we compute the numerical solution for $\hat{c}$ from (4.3). We show the results for two different base states: the asymptotic approximation for the long-time base state used previously in this section, and a numerical solution of (3.1) with well-mixed initial conditions $C(z,0) = 0$. The latter base state differs from the former mainly at early times, where it has a rapidly evolving boundary layer which the former does not. The wave and Marangoni numbers k and Ma are the same as before.

Figure 4.4(a) shows a comparison of the asymptotic amplifications. The results obtained from solutions of (3.1) are labeled "(num)" or "(asy)," respectively, if the numerical solution or the asymptotic approximation for the base state is used. The best agreement is achieved between the improved asymptotic amplification A_{imp} and the numerical solution with the asymptotic base state "$A(t)$ (asy)." The amplifications for the basic approximation is visibly different since it uses only the leading-order approximation for the eigenvalue $\lambda_1^{(0)}$. There is also a discrepancy between the "$A(t)$ (asy)"

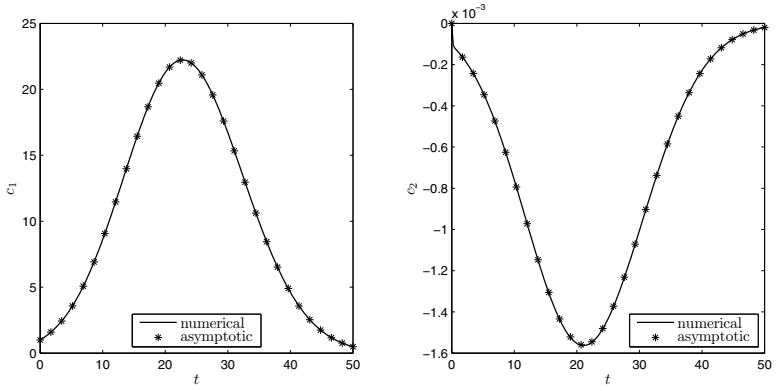

FIG. 4.3. *Comparison of the projections c_1 (left) and c_2 (right) of the numerical solution* (4.3) *with the asymptotic expressions presented in* (4.33).

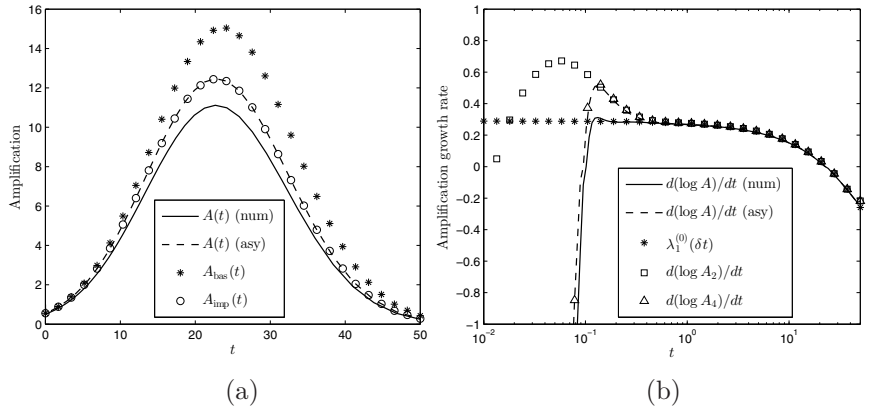

(a) (b)

FIG. 4.4. (a) *A comparison of the asymptotic amplifications with the ones obtained from numerical solutions of* (4.3). *The difference between "$A(t)$ (asy)" and "$A(t)$ (num)" is explained in the text.* (b) *Comparison of the growth rates, i.e., the derivative of the log of the amplifications. Shown are the lines for the growth rates obtained from "$A(t)$ (asy)" and "$A(t)$ (num)" from the basic asymptotic approximation and from the approximations A_N (cf.* (4.35)*) using two and four modes.*

and "$A(t)$ (num)" which reflects the influence of the rapidly evolving boundary layer in the base state.

The initial perturbation (4.34) is not a pure eigenfunction, and thus several $c_l(0)$ (cf. (4.7b)) are nonzero. These are the coefficients of the subdominant modes, which quickly decay relative to the top mode. Therefore, $A(t)$ (asy) and $A_{\rm imp}$ agree well except at early times, where the former includes contributions from the subdominant modes, while the latter does not. The effect of the higher modes is perhaps best seen if we compare asymptotic and numerical growth rates, rather than amplifications, as shown in Figure 4.4(b). At later times, $\lambda_1 = d(\log(A_{\rm bas}))/dt$ agrees very well with both of the numerical growth rates—the difference of $O(\delta)$ is barely visible. At early times, however, the asymptotic growth rate differs from the numerical ones. This difference can be accounted for by including contributions from subdominant

eigenvalues via

$$A_N(t) = \frac{\max_z |\hat{c}_{\mathrm{bas},N}(z,t)|}{\max_z |\hat{c}(z,0)|}, \tag{4.35}$$

where

$$\hat{c}_{\mathrm{bas},N}(z,t) = \sum_{k=1}^{N} c_{ki}^{(0)} v_k^{(0)}(z,\tau) \exp\left[\delta^{-1} \int_0^{\delta t} \lambda_k^{(0)}(\rho)\, d\rho\right],$$

$$c_{ki}^{(0)} = \int_0^1 v_k^{*(0)}(z;0)\, \hat{c}_i(z)\, dz.$$

For $N \geq 4$, the growth rates derived from A_N agree very well with the numerical growth rate "$d(\log(A))/dt$ (asy)" even at early times, where the label "(asy)" has the same meaning as in Figure 4.4(a).

5. Comparison with experiments. We now compare our results to some recent experiments by Bassou and Rharbi [1] using solutions of polystyrene (PS) with a molecular weight of 150 kg/mol in toluene. The mixture was deposited on a glass substrate and then dried in a chamber which was kept at a uniform temperature. The film was observed during the drying process by a variety of visualization techniques to allow for the detection and measurement of convection cells.

The chamber was fitted with lids having holes of different sizes so that the evaporation rate could be controlled. The authors determined the drying rate J by measuring the mass loss of the experiment, and then dividing the measured value by time and the total surface area of the film. Thus, their drying rate corresponds to the right-hand side of (2.5). Specifically, we can set the value J they measure in the first 30 seconds of their experiment approximately equal to the initial value of the right-hand side of (2.5), i.e., $J = k_m c_m$. Expressing δ in terms of J, we get

$$\delta = \frac{J h_i}{D c_m}, \qquad c_m = \beta\rho. \tag{5.1}$$

For the majority of their reported results, the initial drying rate is $3 \times 10^{-4}\,\mathrm{kg/m^2}$ s. Bassou and Rharbi reported that the evaporation rate they measured during "the first 75% of the drying process" remained almost constant for the experiments with evaporation rate $< 3 \times 10^{-4}\,\mathrm{kg/m^2}$ s, and decreased steadily above this value, with a decrease of 15% specifically for the highest evaporation rate ($3.5 \times 10^{-4}\,\mathrm{kg/m^2}$ s). Although they do not state how long the drying process lasts, it seems that for a sizable time, the evaporation rate changes less than linearly with the concentration of the solvent.

The volume fraction is $\beta = 0.85$, and h_i is between 1.4 and 0.15 mm. We follow Bassou and Rharbi and obtain the diffusion constant from measurements by NaNagara et al. [33], although those were carried out for PS with a larger molecular weight. The diffusivity depends on the volume fraction, and by interpolating the data curves we obtain $D = 1.38 \times 10^{-9}\ \mathrm{m^2/s}$ for $\beta = 0.85$. PS and toluene both have a density close to $1000\ \mathrm{kg/m^3}$, so our assumption of a constant density for the liquid mixture seems justified, and we will use the aforementioned value for ρ. We thus have for the thickest film $\delta = 0.36$ and for the thinnest $\delta = 3.8 \times 10^{-2}$, so that we can assume $\delta \ll 1$.

To assess the stability of the liquid film, we also need the Marangoni number Ma introduced in the previous section. Replacing the factor of δ by (5.1) yields

$$\mathrm{Ma} = \frac{(1-\beta)\gamma_c J {h_i}^2}{\mu D^2}. \tag{5.2}$$

The dependence of the surface tension coefficient on the composition of the liquid mixture was measured by Bassou and Rharbi, and the resulting γ_c was found to be 8.5×10^{-7} (N/m)/(mol/m^3). The molar mass of toluene is 92.1×10^{-3} kg/mol, and thus $\gamma_c = 9.2 \times 10^{-6}$ (N/m)/(kg/m^3). The viscosity was given for a number of PS concentrations, and for $\beta = 0.85$ it was $\mu = 0.15$ Pa·s. For the largest initial film thickness $h_i = 1.4$ mm, the Marangoni number is then $\mathcal{M} = 2.9 \times 10^3$, and for the thinnest films $h_i = 0.15$ mm, we obtain $\mathcal{M} = 33$. Thus, the top eigenvalue of the leading-order part of $\mathcal{L}$ suggests that the solutions of (4.3) will, at least initially, have a positive growth rate for a range of wavenumbers if the initial film is sufficiently thick. However, thinner films will have solutions which always decay. The critical initial thickness where $\mathcal{M} = \mathcal{M}_c$ is found to be 0.23 mm. While the prediction agrees with the experimental observations for the thicker films, the thinner films in the experiments were unstable down to 0.15 mm; indications of stabilization were only seen for $h_i \leq 0.1$ mm.

Next we consider the amplification of the perturbation, starting with the experiments with the largest initial film thicknesses. For $\mathcal{M} = 2.9 \times 10^3$, the maximum initial growth rate assuming a fully developed base state is given by the top eigenvalue of $\mathcal{L}_0$ for $k_m = 7.2$ and is $\lambda_m = 2.3 \times 10^2$. To gain three orders of magnitude at this growth rate the perturbation requires a dimensionless time of $t = 3.0 \times 10^{-2} \ll 1$. This contradicts the assumption of a fully developed base state but suggests that the instability will grow very quickly, even before the concentration boundary layer has fully penetrated the film.

We now look at a situation where the perturbation grows more slowly. In the experiment, this is achieved, for example, by reducing the initial film thickness. In fact, as noted before, the smaller film thicknesses used by Bassou and Rharbi correspond to Marangoni numbers close to or even below $\mathcal{M}_c$.

To measure how far we are above criticality, we define

$$\varepsilon(\tau) \equiv \frac{\mathcal{M}(\tau) - \mathcal{M}_c}{\mathcal{M}_c}, \qquad \varepsilon_0 \equiv \varepsilon(0) = \frac{\mathrm{Ma} - \mathcal{M}_c}{\mathcal{M}_c}, \tag{5.3}$$

where $\mathcal{M}$ is given by (4.25) for a fixed choice of Ma; recall that $\mathcal{M}(0) = \mathrm{Ma}$. Here we have emphasized the dependence of both the Marangoni number and of ε on the slow time τ.

Next we expand the eigenvalue $\check{\lambda}_1$ in a Taylor series in terms of $\check{k}$,

$$\check{\lambda}_1 = \varepsilon \check{k}^2 + \left(-\frac{8}{315} + \frac{29}{630}\,\varepsilon + \frac{1}{14}\,\varepsilon^2 \right) \check{k}^4 + O(\check{k}^6). \tag{5.4}$$

By experimentation, we found that for the range of ε we use here, the series converges reasonably fast for $\check{k}$ smaller than about 1.5. From this expansion, we find the following initial leading-order behavior for the cut-off and dominant wavenumber as well as the maximum growth rate, valid for $\varepsilon_0 \ll 1$,

$$\check{k}_c = \frac{3\sqrt{70}}{4}\,\varepsilon_0^{1/2}, \qquad \check{k}_m = \frac{3\sqrt{35}}{4}\,\varepsilon_0^{1/2}, \qquad \check{\lambda}_{1m} = \frac{315}{32}\,\varepsilon_0^2, \tag{5.5}$$

respectively. An obvious choice for the initial ε_0 and thus the Marangoni number would be to let $\varepsilon_0 = \delta^{1/2}$, so that $\check{\lambda}_{1m} = O(\delta)$ in the beginning. However, the eigenvalue will change its sign as the line $\check{\lambda}_1 = 0$ is approached, and this happens so quickly that the amplification achieved at this time is very small. Moreover, if $\check{\lambda}_1 = O(\delta)$, then $\check{\lambda}_1/\delta$ is of the same order as the terms neglected in the integral I for c_{bas} (cf. (4.28)), making estimates of the maximum amplification inaccurate. (Note, however,

that our arguments here rely on orders of magnitude of the amplification, which will be small in this situation with our without higher corrections to I.) Therefore, we will consider $\varepsilon_0 \gg \delta^{1/2}$.

We determine the amplification by evaluating, for fixed k and Ma, the integral I in (4.28). Letting $\varepsilon = (1 + (\eta - 1)/\beta)(1 + \varepsilon_0) - 1$ and $\check{k} = \eta k$ in (5.4) (with enough terms to ensure accuracy), we obtain an expression that can be plugged into I. In principle, this yields an explicit result, but the algebra and resulting expressions are tedious and were handled by using Maple. We therefore only report the numerical results for a couple of specific choices of parameters. As before, we use $\beta = 0.85$.

We start with a small value for $\varepsilon_0 = 0.1$ and $k = 1.0$. As expected, I first increases as the thickness $h_0 < 1$ decreases until it reaches a maximum of $I = 2.2 \times 10^{-3}$, after which it decays and eventually becomes negative. Other choices of k produced values for I that were equal to or less than this value. The amplification that results from this is $\exp(I/\delta)$. If we assume that we need at least three orders of magnitude to amplify a perturbation so that it becomes visible in an experiment, we find that $\delta < 2.2 \times 10^{-3}/7 \approx 3 \times 10^{-4}$. Even if we relax our assumption and consider a factor of ten to be enough to create a visible pattern, this increases the threshold for δ only by a factor of three which is still less than even the smallest δ reported by Bassou and Rharbi. Thus it seems unlikely that visible convection cells will show up.

These values have also been verified by solving the eigenvalue problem and the full linear problem numerically. More specifically, the top eigenvalue $\check{\lambda}_1$ was computed for various values of the film thickness, and the integral I was evaluated using Gaussian quadrature. The maximum value was found to be $I = 2.2 \times 10^{-3}$, in accordance with the above result. Moreover, the corresponding amplification at this critical thickness and when $\delta = 3 \times 10^{-4}$ was found to be $A_{\text{bas}} = 1.6 \times 10^3$. This is of the same order of magnitude as the predicted amplification, the difference being a result of neglecting the prefactors in (4.28). Because of the time dependence of the top eigenfunction in (4.28), the time at which the maximum amplification occurs does not coincide exactly with the time when I attains its maximum. However, we find that the maximum amplification actually matches A_{bas}, that is, $\max_t A(t) = 1.6 \times 10^3$.

Repeating the investigation with $\varepsilon_0 = 0.5$ (i.e., Ma = 120) and $k = 1.5$, we obtain $I = 0.15$. This matches the numerical value of I that is computed using the procedure described above. A sufficient amplification of three orders of magnitude would require $\delta < 0.02$. An initial Marangoni number of 120 is achieved with a film thickness of 0.287 mm and for this thickness, $\delta = 0.073$, well above the required value. The amplification achieved for this δ would be only about $\exp(0.15/0.073) < 10$, making it again unlikely that any manifestation of the instability can be seen even though the initial Ma is 50% above $\mathcal{M}_c$. Numerical simulations support these claims. The amplifications that are achieved when $\delta = 0.02$ are $A_c = \max_t A(t) = 2.4 \times 10^3$, where A_c denotes the amplification when I attains its maximum. When $\delta = 0.073$, we find $A_c = \max_t A(t) = 11$. All of these values are of the same order of magnitude as the predicted amplifications.

The expansion in (5.4) fails to converge for $\varepsilon_0 = 0.50$ and $k > 3/2$. Therefore, we use numerical solutions to study the amplification of perturbations with wavenumbers that are larger than this value. We find that the maximum value of I over all of the wavenumbers is $\max_k I(k) = 0.17$, which is achieved when $k = 1.80$. Since these optimal values are close to values of k and I from the last paragraph, we conclude that the previous discussion is representative of dynamics when Ma = 120.

In summary, the theory predicts films which are more stable than those actually

observed in the experiments. This is particularly true for thinner films, and we now discuss possible reasons. One assumption that has been made is that the system is isothermal. That is, temperature variations in the fluid have been neglected. It is well known, however, that the evaporation of solvent will lead to a cooling of the air-liquid interface, thus inducing a temperature gradient in the fluid. This, in turn, can lead to the onset of convection rolls through thermal-buoyancy-driven and thermocapillary-driven instabilities. Estimates of the relevant dimensionless numbers suggest that thermal-buoyancy-driven convection can be ruled out as the dominant driving mechanism of the instability, since the thermal Rayleigh numbers are always very small (about 10 or less) compared to typical critical values (around 1000). The thermal Marangoni numbers are also small for thinner films compared to the typical range of critical values (less than 24 for $h_i < 0.5$ mm) and only get close to them for the thickest films (about 67 for $h_i = 1.4$ mm). However, since convection brings up both solvent-rich and hotter liquid, which both lower the surface tension, the two Marangoni effects could add up and thus reinforce each other. Solutal buoyancy effects may play a role for the thicker films but not for the thinner ones. For $h_i = 1.4$ mm the solutal Rayleigh number is around 1080, but for $h_i < 0.5$ mm it is less than 18, well below the typical range of critical values in buoyancy-driven convection.

Another aspect of the model that needs to be revisited is our use of a one-layer model for the liquid with constant mass transfer coefficients at the interface and zero solvent vapor concentration far away from the surface. A two-layer model has been investigated, for example, by Machrafi et al. [30] for an evaporating water-ethanol film. An approximate expression for the critical Marangoni number (from a "frozen-time" analysis) is given in equations (75) and (113) of this reference. We tried several choices of the parameters—for water-ethanol films with varying total thickness of the liquid-gas layers, and also for toluene-polystyrene films—and found that where the two critical Marangoni numbers differed visibly, the one for the two-layer case was larger. This suggests that the coupling with the gas phase in the model we use here will likely raise rather than lower the critical Marangoni threshold and make the system for the thinner films even more stable.

6. Conclusions. In this paper, we have investigated the stability of a thin layer of a mixture that is composed of a volatile solvent and a nonvolatile polymer. The evaporation of the solvent induces a concentration gradient, which in turn leads to Marangoni stresses that can drive a Bénard–Marangoni-type instability if the surface tension at the liquid/gas interface increases with the polymer concentration. For a simplified model, we determine the base state and then linearize about this base state to determine its stability.

In contrast to classical Bénard–Marangoni convection, where the liquid layer is heated from below and the Marangoni stresses arise from the temperature dependence of surface tension, the base state is itself time dependent since the loss of solvent leads to a slow change in the film thickness and composition. Thus, the linearized system is not autonomous. We address this issue by first projecting the initial value problem onto the leading eigenmodes and then deriving multiple-scale expansions for the solution of the resulting ODE system. These make use of the fact that the evaporation is slow on the diffusive time scale which governs the potential instability, encapsulated by a small Biot number δ. We determine both the leading-order result and the first correction. The latter reveals that a necessary condition for the validity of the expansions is that the eigenvalues of the spatial operator remain well separated. We expect that a sufficient distance of the top eigenvalue from the rest of the spectrum

is particularly important. On the other hand, the absolute value of the eigenvalues is not relevant for the validity of the expansions.

From the multiple-scale expansions, we derive two approximations for the amplification of the top-mode contribution to an initial perturbation (noticing that the subdominant modes will be irrelevant for all but very early times). The first, or basic, approximation uses only the leading-order (in δ) part of all the contributions in the expansions. Thus, the argument of the exponential factor contains only the leading-order approximation to the eigenvalue. The second uses in particular the full eigenvalue and also includes the "self-coupling" term γ_{11}.

The improved approximation is substantially more accurate than the basic one, but the latter is more readily obtained, so we rely on it to investigate the experiments by Bassou and Rharbi. Specifically, we use it to predict the maximum amplification a perturbation achieves before the system restabilizes. It turns out that only very modest amplifications are achieved unless the initial Marangoni number is more than 50% above the critical Marangoni number $\mathcal{M}_c = 80$ obtained from the leading-order-in-δ operator.

It is interesting to compare our results with those obtained for models where only the effect of latent heat due to evaporation is included, such as, for example, in the work by Doumenc et al. [15]. It turns out that for thick enough films, both thermal-buoyancy and thermocapillary effects destabilize the film. For smaller thicknesses, only thermocapillarity plays a role, while the thinnest films are stable with respect to both effects. For solutal instabilities such as treated in our work, the basic ordering of the buoyancy and soluto-capillary effects are similar. However, in the thermal case, the attention is mainly focused on instabilities that arise during the initial transient of the base state (before the temperature gradient has reached the bottom of the liquid layer), and therefore the change of the film thickness can be neglected. We are not aware that a similar study has been carried out for the solutal effect. In contrast, our work focuses on the long-time regime where the base state evolves only on the slow time scale of the mass loss due to evaporation. Both the change in the concentration and the decrease of the film thickness need to be included in the stability analysis.

Appendix. In this appendix, we identify and solve the solvability condition that is required to fully determine the first-order corrections $d_1^{(1)}$ and $d_2^{(1)}$. We first integrate (4.18),

$$d_1^{(1)}(T,\tau) = -\frac{\gamma_{12}^{(0)}(\tau)}{\lambda^{(0)}(\tau)}\exp(-T)c_{2i}^{(0)} + a_1(\tau), \tag{A.1a}$$

$$d_2^{(1)}(T,\tau) = \frac{\gamma_{21}^{(0)}(\tau)}{\lambda^{(0)}(\tau)}\exp(T)c_{1i}^{(0)} + a_2(\tau). \tag{A.1b}$$

The ODE system for the second-order correction problem is

$$\begin{aligned} d_{1,T}^{(2)}(T,\tau) = {} & \frac{\gamma_{12}^{(0)}(\tau)}{\lambda^{(0)}(\tau)}\exp(-T)d_2^{(1)}(T,\tau) \\ & + \left[\frac{\gamma_{12}^{(1)}(\tau)}{\lambda^{(0)}(\tau)} - \frac{\gamma_{12}^{(0)}(\tau)}{(\lambda^{(0)}(\tau))^2}\left(\lambda^{(1)}(\tau)+\gamma^{(0)}(\tau)\right)\right]\exp(-T)d_2^{(0)}(\tau) \\ & - \frac{d_{1,\tau}^{(1)}(\tau)}{\lambda^{(0)}(\tau)}, \end{aligned} \tag{A.2a}$$

$$d_{2,T}^{(2)}(T,\tau) = \frac{\gamma_{21}^{(0)}(\tau)}{\lambda^{(0)}(\tau)}\exp(T)d_1^{(1)}(T,\tau) + \left[\frac{\gamma_{21}^{(1)}(\tau)}{\lambda^{(0)}(\tau)} - \frac{\gamma_{21}^{(0)}(\tau)}{(\lambda^{(0)}(\tau))^2}\left(\lambda^{(1)}(\tau)+\gamma^{(0)}(\tau)\right)\right]\exp(T)d_1^{(0)}(\tau) - \frac{d_{2,\tau}^{(1)}(\tau)}{\lambda^{(0)}(\tau)}. \tag{A.2b}$$

Inserting (4.19) and (A.1) into (A.2) and identifying the terms on the right-hand sides that may lead to secular terms (the ones that do not have a prefactor $\exp(T)$ and $\exp(-T)$) yields the solvability conditions

$$a_{1,\tau} = \frac{\gamma_{12}^{(0)}(\tau)\gamma_{21}^{(0)}(\tau)}{\lambda^{(0)}(\tau)}c_{1i}^{(0)}, \qquad a_{2,\tau} = -\frac{\gamma_{12}^{(0)}(\tau)\gamma_{21}^{(0)}(\tau)}{\lambda^{(0)}(\tau)}c_{2i}^{(0)}, \tag{A.3a}$$

with initial conditions arising from (4.18c),

$$a_1(0) = \frac{\gamma_{12}^{(0)}(0)}{\lambda^{(0)}(0)}c_{2i}^{(0)} + c_{1i}^{(1)}, \qquad a_2(0) = -\frac{\gamma_{21}^{(0)}(0)}{\lambda^{(0)}(0)}c_{1i}^{(0)} + c_{2i}^{(1)}. \tag{A.3b}$$

We solve these equations for a_1 and a_2 and insert the result into (A.1),

$$d_1^{(1)}(T,\tau) = -\frac{\gamma_{12}^{(0)}(\tau)}{\lambda^{(0)}(\tau)}\exp(-T)c_{2i}^{(0)} + c_{1i}^{(0)}\int_0^\tau \frac{\gamma_{12}^{(0)}(\rho)\gamma_{21}^{(0)}(\rho)}{\lambda^{(0)}(\rho)}d\rho + \frac{\gamma_{12}^{(0)}(0)}{\lambda^{(0)}(0)}c_{2i}^{(0)} + c_{1i}^{(1)}, \tag{A.4a}$$

$$d_2^{(1)}(T,\tau) = \frac{\gamma_{21}^{(0)}(\tau)}{\lambda^{(0)}(\tau)}\exp(T)c_{1i}^{(0)} - c_{2i}^{(0)}\int_0^\tau \frac{\gamma_{12}^{(0)}(\rho)\gamma_{21}^{(0)}(\rho)}{\lambda^{(0)}(\rho)}d\rho - \frac{\gamma_{21}^{(0)}(0)}{\lambda^{(0)}(0)}c_{1i}^{(0)} + c_{2i}^{(1)}. \tag{A.4b}$$

Acknowledgments. The authors would like to thank Chris Breward, Colin Please, and Barbara Wagner for many helpful discussions.

REFERENCES

[1] N. Bassou and Y. Rharbi, *Role of Bénard-Marangoni instabilities during solvent evaporation in polymer surface corrugations*, Langmuir, 25 (2009), pp. 624–632.
[2] H. Bénard, *Les tourbillons cellulaires dans une nappe liquide*, Revue Générale des Sciences, 11 (1900), pp. 1261–1271, 1309–1328.
[3] H. Bénard, *Les tourbillons cellulaires dans une nappe liquide transportent de la chaleur par convection en régime permanent*, Annales de Chimie Physique, 7 (1901), pp. 62–145.
[4] H. Bénard, *Les tourbillons cellulaires dans une nappe liquide: Méthodes optiques d'observation et d'enregistrement*, Journal de Physique Théorique et Appliquée, 10 (1901), pp. 254–266.
[5] B. S. Bhadauria and P. K. Bhatia, *Time-periodic heating of Rayleigh-Benard convection*, Phys. Scripta, 66 (2002), pp. 59–65.
[6] M. J. Block, *Surface tension as the cause of Bénard cells and surface deformation in a liquid film*, Nature, 178 (1956), pp. 650–651.
[7] E. Bodenschatz, W. Pesch, and G. Ahlers, *Recent developments in Rayleigh-Bénard convection*, in Annual Review of Fluid Mechanics, Vol. 32, Annual Reviews, Palo Alto, CA, 2000, pp. 709–778.
[8] E. Bormashenko, S. Balter, R. Pogreb, Y. Bormashenko, O. Gendelman, and D. Aurbach, *On the mechanism of patterning in rapidly evaporated polymer solutions: Is temperature-gradient-driven Marangoni instability responsible for the large-scale patterning?*, J. Colloid Interface Sci., 343 (2010), pp. 602–607.

[9] D. E. Bornside, C. W. Macosko, and L. E. Scriven, *Spin coating: One-dimensional model*, J. Appl. Phys., 66 (1989), pp. 5185–5193.
[10] M. Bouthier, *Stabilité linéaire des écoulements presque parallèlles*, J. Mécanique, 11 (1972), pp. 599–621.
[11] M. Bouthier, *Stabilité linéaire des écoulements. Partie* II. *La couche limite de Blasius*, J. Mécanique, 12 (1973), pp. 75–95.
[12] P. Colinet, J. C. Legros, and M. G. Velarde, *Nonlinear Dynamics of Surface-Tension-Driven Instabilities*, Wiley-VCH, Berlin, 2001.
[13] I. G. Currie, *The effect of heating rate on the stability of stationary fluids*, J. Fluid Mech., 29 (1967), pp. 337–347.
[14] S. H. Davis, *Thermocapillary instabilities*, in Annual Review of Fluid Mechanics, Vol. 19, Annual Reviews, Palo Alto, CA, 1987, pp. 403–435.
[15] F. Doumenc, T. Boeck, B. Guerrier, and M. Rossi, *Transient Rayleigh–Bénard–Marangoni convection due to evaporation: A linear non-normal stability analysis*, J. Fluid Mech., 648 (2010), pp. 521–539.
[16] B. D. Edmonstone, R. V. Craster, and O. K. Matar, *Surfactant-induced fingering phenomena beyond the critical micelle concentration*, J. Fluid Mech., 564 (2006), pp. 105–138.
[17] T. D. Foster, *Stability of a homogeneous fluid cooled uniformly from above*, Phys. Fluids, 8 (1965), pp. 1249–1257.
[18] M. G. Hennessy, *Organic Solar Cells and the Marangoni Instability*, transfer thesis, University of Oxford, 2011.
[19] S. Y. Heriot and R. A. L. Jones, *An interfacial instability in a transient wetting layer leads to lateral phase separation in thin spin-cast polymer-blend films*, Nat. Mater., 4 (2005), pp. 782–786.
[20] G. M. Homsy, *Global stability of time-dependent flows: Impulsively heated or cooled fluid layers*, J. Fluid Mech., 60 (1973), pp. 129–139.
[21] S. D. Howison, J. A. Moriarty, J. R. Ockendon, E. L. Terrill, and S. K. Wilson, *A mathematical model for drying paint layers*, J. Engrg. Math., 32 (1997), pp. 377–394.
[22] B. S. Jhaveri and G. M. Homsy, *The onset of convection in fluid layers heated rapidly in a time-dependent manner*, J. Fluid Mech., 114 (1982), pp. 251–260.
[23] K. H. Kang and C. K. Choi, *A theoretical analysis of the onset of surface-tension-driven convection in a horizontal liquid layer cooled suddenly from above*, Phys. Fluids, 9 (1997), pp. 7–15.
[24] J. Kevorkian, *Perturbation techniques for oscillatory systems with slowly varying coefficients*, SIAM Rev., 29 (1987), pp. 391–461.
[25] J. Kevorkian and J. D. Cole, *Multiple Scale and Singular Perturbation Methods*, Appl. Math. Sci. 14, Springer, New York, 1996.
[26] J. R. King, A. Münch, and B. A. Wagner, *Linear stability analysis of a sharp-interface model for dewetting thin films*, J. Engrg. Math., 63 (2008), pp. 177–195.
[27] W. Lick, *The instability of a fluid layer with time-dependent heating*, J. Fluid Mech., 21 (1965), pp. 565–576.
[28] C. C. Lin, *Some mathematical problems in the theory of the stability of parallel flows*, J. Fluid Mech., 10 (1961), pp. 430–438.
[29] H. Machrafi, A. Rednikov, P. Colinet, and P. C. Dauby, *Bénard instabilities in a binary-liquid layer evaporating into an inert gas: Stability of quasi-stationary and time-dependent reference profiles*, Eur. Phys. J. Special Topics, 192 (2011), pp. 71–81.
[30] H. Machrafi, A. Rednikov, P. Colinet, and P. C. Dauby, *Bénard instabilities in a binary-liquid layer evaporating into an inert gas*, J. Colloid Interface Sci., 349 (2010), pp. 331–353.
[31] E. G. Mahler and R. S. Schechter, *The stability of a fluid layer with gas absorption*, Chem. Engrg. Sci., 25 (1970), pp. 955–968.
[32] A. Münch and B. Wagner, *Impact of slippage on the morphology and stability of a dewetting rim*, J. Phys. Condensed Matter, 23 (2011), 184101.
[33] B. NaNagara, R. D. O'Connor, and F. D. Blum, *Mobility of toluene in polystyrene-toluene solutions: A NMR study*, J. Phys. Chem., 96 (1992), pp. 6417–6423.
[34] A. A. Nepomnyashchy, I. B. Simanovskii, and J. C. Legros, *Interfacial Convection in Multilayer Systems*, Springer Monographs in Mathematics, Springer, New York, 2006.
[35] J. R. A. Pearson, *On convection cells induced by surface tension*, J. Fluid Mech., 4 (1958), pp. 489–500.
[36] Lord Rayleigh, *On convection currents in a horizontal layer of fluid, when the higher temperature is under side*, Philos. Mag., 32 (1916), pp. 529–546.
[37] S. Rosenblat and G. A. Tanaka, *Modulation of thermal convection instability*, Phys. Fluids, 14 (1971), pp. 1319–1322.

[38] J. W. Scanlon and L. A. Segel, *Finite amplitude cellular convection induced by surface tension*, J. Fluid Mech., 30 (1967), pp. 149–162.
[39] P. J. Schmid and D. S. Henningson, *Stability and Transition in Shear Flows*, Springer, New York, 2001.
[40] L. E. Scriven and C. V. Sternling, *On cellular convection driven by surface-tension gradients: Effects of mean surface tension and surface viscosity*, J. Fluid Mech., 19 (1964), pp. 321–340.
[41] S. F. Shen, *Some considerations on the laminar stability of time-dependent basic flows*, J. Aerospace Sci., 28 (1961), pp. 397–404, 417.
[42] K. A. Smith, *On convective instability induced by surface-tension gradients*, J. Fluid Mech., 24 (1966), pp. 401–414.
[43] L. B. Smolka and T. P. Witelski, *On the planar extensional motion of an inertially driven liquid sheet*, Phys. Fluids, 21 (2009), 042101.
[44] M. Souche and N. Clarke, *Interfacial instability in bilayer films due to solvent evaporation*, Eur. Phys. J. E, 28 (2009), pp. 47–55.
[45] O. Touazi, E. Chénier, F. Doumenc, and B. Guerrier, *Simulation of transient Rayleigh-Bénard-Marangoni convection induced by evaporation*, Internat. J. Heat Mass Transfer, 53 (2010), pp. 656–664.
[46] G. Toussaint, H. Bodiguel, F. Doumenc, B. Guerrier, and C. Allain, *Experimental characterization of buoyancy- and surface tension-driven convection during the drying of a polymer solution*, Internat. J. Heat Mass Transfer, 51 (2008), pp. 4228–4237.
[47] B. Trouette, E. Chénier, C. Delcarte, and B. Guerrier, *Numerical study of convection induced by evaporation in cylindrical geometry*, Eur. Phys. J. Special Topics, 192 (2011), pp. 83–93.
[48] J. S. Vrentas and C. M. Vrentas, *Exchange of stabilities for surface tension driven convection*, Chem. Engrg. Sci., 59 (2004), pp. 4433–4436.
[49] M. R. E. Warner, R. V. Craster, and O. K. Matar, *Unstable van der Waals driven line rupture in Marangoni driven thin viscous films*, Phys. Fluids, 14 (2002), pp. 1642–1654.